GA–A22404

CHARACTERIZATION OF CORE IMPURITY TRANSPORT AND ACCUMULATION IN VARIOUS OPERATING REGIMES IN DIII–D

by
M.R. WADE, D.G. WHYTE, R.D. WOOD, and W.P. WEST

JULY 1996

GA–A22404

CHARACTERIZATION OF CORE IMPURITY TRANSPORT AND ACCUMULATION IN VARIOUS OPERATING REGIMES IN DIII–D

by
M.R. WADE,* D.G. WHYTE,† R.D. WOOD,Δ and W.P. WEST

This is a preprint of a paper to be presented at the Twenty-Third European Conference on Controlled Fusion and Plasma Physics, June 24–28, 1996, Kiev, Ukraine, and to be published in *The Proceedings.*

*Oak Ridge National Laboratory, Oak Ridge, Tennessee.
†INRS — Energie et Materiaux, Varennes, Quebec, Canada.
ΔLawrence Livermore National Laboratory, Livermore, California.

Work supported by
the U.S. Department of Energy
under Contract Nos. DE-AC03-89ER51114, W-7405-ENG-48
DE-AC05-96OR22464, and Grant Nos. DE-FG03-85ER53266
and DE-FG02-89ER53297

GA PROJECT 3466
JULY 1996

CHARACTERIZATION OF CORE IMPURITY TRANSPORT AND ACCUMULATION IN VARIOUS OPERATING REGIMES IN DIII–D*

M.R. Wade,† D.G. Whyte,Δ R.D. Wood,◊ and W.P. West
General Atomics, P.O. Box 85608, San Diego, California 92186-9784 USA

Impurity contaminants in the core plasma of future burning devices such as the International Thermonuclear Experimental Reactor (ITER) are inevitable and will undoubtedly have a deleterious effect on plasma performance. Unfortunately, because of the limited amount of information available, the models presently being used to predict ITER performance simply assume a flat concentration profile for all impurities with an ad hoc concentration chosen for each impurity. In an attempt to start closing the gap between present experimental data and these models, experiments have been conducted on DIII–D with particular emphasis placed on 1) characterizing the buildup of intrinsic impurities in the plasma core in various confinement and divertor regimes, 2) measuring the steady-state impurity (both intrinsic and seeded) density profiles in various operating regimes, and 3) determining whether impurity transport properties are dependent on the charge (or mass) of the impurity. The primary focus of these studies has been on characterizing impurity buildup in a wide variety of operating conditions in ELMing H–mode plasmas. However, enhanced confinement regimes such as ELM-free H–mode, VH–mode, and the negative central shear (NCS) regime offer the potential of a more attractive reactor scenario. Since the degree of impurity accumulation will have a significant impact on the attractiveness of these regimes, studies have also been conducted to characterize impurity buildup in these regimes.

In the present configuration of DIII–D in which graphite tiles cover ~90% of the plasma facing surface, spectroscopic surveys show carbon to be the dominant impurity with the core carbon concentration typically between 1%–3% of the electron density. These studies are made possible by the ability to accurately measure carbon density profiles on DIII–D using active charge-exchange recombination (CER) spectroscopy.[1] In most DIII–D plasmas, carbon is fully stripped over the majority of the plasma cross section, and therefore the total inventory of carbon can be computed directly, thereby alleviating uncertainties associated with transport modeling that is generally required to determine the charge-state distribution.

Impurity Behavior in L-mode and ELMing H-Mode Plasmas

In both L–mode and ELMing H–mode plasmas, the carbon inventory reaches steady-state shortly after the onset of the mode, provided other plasma parameters (e.g., injected power, magnetic equilibrium, plasma density, etc.) are maintained constant. This is similar to previously reported observations of high-Z impurity behavior in DIII–D.[2] The steady-state carbon concentration (relative to the electron density) profile is flat in both L–mode and ELMing H–mode. Presently, analysis is in progress to provide a complete survey of carbon buildup in a variety of operating conditions in L–mode and ELMing H–mode plasmas. Although this survey is incomplete, several interesting phenomena have been observed to date. Of particular interest to ITER are data from power scans and radiative divertor discharges which suggest that the core carbon content is not necessarily directly related to the heat/particle flux incident on the divertor target. Table 1 summarizes data of interest from a set of attached divertor, ELMing H–mode discharges in which the injected beam power was systematically increased from 3 MW to 9 MW. As expected, the increase in beam power resulted in a concomitant increase in the total conducted power to the divertor target. One would expect that such an increase in the heat flux would result in an increase in target erosion and carbon influx to the divertor plasma. This expectation is verified by inference of the divertor carbon density from measurements via a SPRED UV instrument viewing the divertor plasma which indicate that the carbon density increases by a factor of 2 as the power is increased from 3 to 9 MW. However, measurements of the core carbon content via CER show the content decreases as the input power is increased. Such a trend suggests that the divertor and

*Work supported by the U.S. Department of Energy under Contract Nos. DE-AC03-89ER51114, DE-AC05-96OR22464, and W-7405-ENG-48.
†Oak Ridge National Laboratory, Oak Ridge, Tennessee.
ΔINRS — Energie et Materiaux, Varennes, Quebec, Canada.
◊Lawrence Livermore National Laboratory, Livermore, California.

SOL plasma becomes more efficient in screening impurities from the core plasma as the input power is increased. One possible mechanism for this improvement is an increase in the ELM frequency as the input power is increased. Since previous studies have shown that ELMs are effective in sweeping impurities out of the edge plasma , it is likely that an increased frequency of ELMs leads to better screening of impurities. The data shown in Table 1 is consistent with this hypothesis as the ELM frequency increases in these discharges from 40 Hz to 150 Hz as the input power is increased. However, since there are several other possible mechanisms for this improvement (e.g., improved ionization potential of the divertor plasma, increased particle flow toward divertor target thereby entraining the impurities, better, etc.), detailed modeling (including modeling of the carbon sources) is requited to determine the primary mechanism responsible for this trend.

Table 1. Selected Parameters During an Input Power Scan

Input power (MW)	8.9	6.2	3.1
Line-averaged density ($\times 10^{19}$ m^{-3})	6.0	6.0	6.2
Separatrix density ($\times 10^{19}$ m^{-3})	2.0	1.8	2.0
Separatrix temperature (eV)	90	80	75
Total heat flux to divertor (MW)	3.9	3.1	1.6
ELM frequency (Hz)	150	140	40
Core carbon content ($\times 10^{19}$ particles)	1.0	1.2	1.8
Carbon concentration at $\rho = 0.7$ (%)	0.9	0.95	1.5

Over the past several years, several modes of operations have been demonstrated on DIII–D in which the peak heat flux to the divertor target has been reduced by a factor of 5 through controlled gas injection of either deuterium, neon, or nitrogen.[3,4] Given this large reduction in heat flux to the divertor target, one might expect a similar decrease in the core carbon content. Because the formation of radiative divertor conditions in DIII–D are accompanied by increases in the plasma density, systematic comparisons between the detached and attached cases are difficult. The comparisons made here take advantage of the fact that gas injection to form radiative divertor conditions generally begins subsequent to the high-power phase and H–mode formation. This allows measurement of the evolution of the carbon content from the attached divertor phase into the heat flux reduction phase. Such analysis shows that in the deuterium injection case the core inventory of carbon to be ~20% larger while the fuel dilution due to carbon remains essentially the same due to a similar increase in the plasma electron density. In the neon injection case, a large reduction (~ a factor of 2) in the core carbon inventory and fuel dilution due is observed even though the additional neon radiation in the core reduces the ELM frequency from ~60 Hz to 10 Hz. However, because of the additional influx of neon impurities, the core Z_{eff} increases substantially from 1.5 to 3.0. In the nitrogen injection cases, the core inventory of carbon increases by approximately 50% and the fuel dilution due to carbon increases by ~25%. The difference between Ne injection and either D_2 or N_2 injection suggests chemical sputtering of carbon in the deuterium and nitrogen cases may play an important role in the total carbon sputtering rate, but further studies (including detailed modeling) are required to determine the predominant mechanisms in these cases.[5]

Impurity Behavior in Enhanced Confinement Regimes

In enhanced confinement regimes such as ELM-free H–mode, VH–mode,[6] and NCS discharges,[7] the carbon inventory evolution is somewhat more complicated. In ELM-free H–mode plasmas, the carbon inventory increases monotonically throughout the ELM-free phase. The carbon density and concentration increases over the entire profile at equal rates until late in the discharge when central accumulation occurs. This central accumulation leads to increased radiation and eventually to loss of H–mode confinement. This observation is consistent with previous observations on DIII–D and other tokamaks with regard to impurity accumulation in ELM-free H–mode plasmas. In VH–mode plasmas, the total carbon content in VH–mode plasmas is observed to increase approximately linearly with time throughout the entire VH–mode phase (see Fig. 1). In some cases, the electron source rate from this influx (9×10^{20} s^{-1}) exceeds the beam source rate by a factor of ~2–3. In contrast to the ELM-free H–mode results, this influx of carbon primarily accumulates in the plasma periphery (near $\rho = 0.8$), resulting in carbon concentration profiles that get progressively more hollow throughout the VH–mode phase. Typically, this leads to an edge Z_{eff} (computed assuming carbon to the only impurity) near 4.0 (~6.0 in some extreme cases) while the plasma core remains relatively clean with $Z_{eff} \sim 1.5$. Since the carbon density profile does not reach equilibrium during the short extent of the VH–mode phase, it is not possible to determine *a priori* from this data whether such a hollow profile is inherent to the VH–mode or

is primarily due to the transient nature of the measurement. Transport studies designed to elucidate the intrinsic transport properties of VH–mode as well as L–mode and ELMing H–mode are described in more detail in Section III.

The carbon behavior in NCS discharges appears to be dependent on whether the edge plasma exhibits an L–mode or H–mode character. The evolution of a typical NCS discharge is shown in Fig. 2. As is typical of NCS plasmas, the target plasma is produced by the application of an early beam during the plasma current ramp-up phase. In this particular discharge, the edge plasma exhibits an L–mode character (shallow gradients in density and temperature) from the initiation of beam injection to 2.25 s. At 1.9 s, the input power is raised to 8.0 MW and a transport barrier forms in the core plasma near $\rho = 0.4$ as evidenced by a rapid increase in the core ion temperature. The carbon density in the core plasma is also observed to increase during this phase while the edge carbon density remains nearly constant. The simultaneous increase in the core electron density and the impurity density results in a carbon concentration (and Z_{eff}) that changes little during this phase. Also, it is observed that the carbon inventory increases only slightly throughout the L–mode phase. At ~2.25 s, the edge plasma undergoes a transition and begins to exhibit an H–mode character (sharp gradients in density and temperature). Subsequent to this transition, the carbon inventory increases linearly throughout the remainder ELM-free portion of this phase. As in the VH–mode case, this carbon influx primarily accumulates in the plasma edge with impurity concentrations on the order of 6%–10% quickly achieved while the core plasma remains relatively clean ($f_C < 3\%$). Discharges in which NCS has been maintained simultaneously with ELMs exhibit a clamping and subsequent decrease in the carbon concentration once ELMs begin, similar to what is observed in ELMing H–mode plasmas.

From this set of data, it is clear that enhanced confinement regimes with edge plasmas which exhibit an H-mode edge (ELM-free H–mode, VH–mode, and NCS H–mode) are susceptible to impurity buildup to the extent that calls into question their suitability for a reactor. Clearly, some means of controlling impurity buildup is required. In the case of ELM-free H–mode and NCS H–mode, ELMs have been

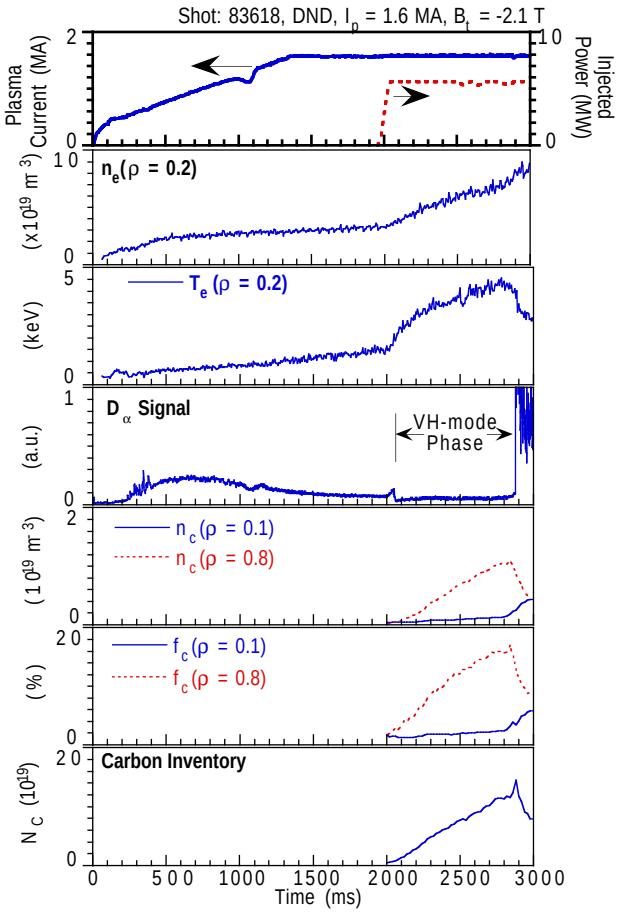

Fig. 1. Selected waveforms for a VH–mode discharge.

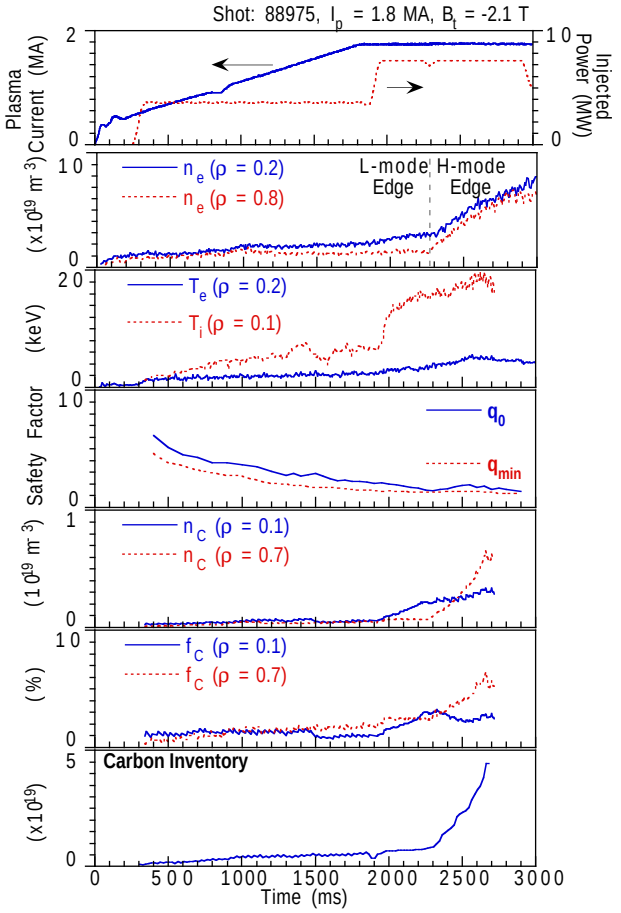

Fig. 2. Selected waveforms for a NCS discharge.

From this set of data, it is clear that enhanced confinement regimes with edge plasmas which exhibit an H-mode edge (ELM-free H–mode, VH–mode, and NCS H–mode) are susceptible to impurity buildup to the extent that calls into question their suitability for a reactor. Clearly, some means of controlling impurity buildup is required. In the case of ELM-free H–mode and NCS H–mode, ELMs have been shown to be effective in reducing the rate of carbon buildup. In this regard, the benefit of ELMs in controlling the impurity levels in these confinement regimes likely outweighs the loss in energy confinement associated with the ELMs.

Low-Z Impurity Transport

As discussed above, distinct differences in the measured steady-state profiles of various low-Z impurities have been observed as the confinement mode changes. In L–mode and in ELMing H–mode plasmas, the concentration profiles of helium, neon, and carbon are all similar to the electron density profile. However, in VH–mode plasmas, the helium density profile continues to mimic the electron density whereas the carbon and neon profiles are distinctly hollow. To address these obvious differences in transport behavior of low-Z impurities, experiments to determine the transport coefficients (namely, particle diffusivity and convective velocity) have been carried out by introducing perturbative gas puffs of helium, nitrogen, and neon in L–mode, ELMing H–mode, and VH–mode plasmas. The evolution of impurity density profile subsequent to the gas puff is followed using the DIII–D CER system with a time resolution of 5 ms. To deduce transport coefficients, the impurity particle flux Γ_Z is determined from the continuity equation. Assuming the impurity flux is be made up of diffusive and convective flows, the relevant transport coefficients (namely, the diffusivity D_Z and the convective velocity V_Z) are determined by using a linear regression analysis of the normalized flux Γ_Z/n_Z and the normalized density gradient $\nabla n_Z/n_Z$.[8,9] The results of such analysis are shown in Fig. 3, where the diffusivity and pinch velocity for helium and neon is compared for both L–mode and VH–mode plasmas. It is found that in L–mode plasmas, the transport of helium and neon is essentially the same. The lack of a Z-dependence in L–mode plasmas suggests that impurity transport is dominated by anomalous processes in this regime. However, in VH–mode plasmas, there is a substantial difference in the transport properties of helium and neon. Although the diffusivity for both helium and neon are nearly the same, the convective velocity is nearly equal and opposite in magnitude in the two cases. This observed Z-dependence is suggestive of neoclassical-like impurity transport, in which a strong Z-dependence is expected. Note that the L–mode and VH–mode regimes are also characterized by substantial differences in plasma rotation. Work is in progress to compare this data to neoclassical predictions including plasma rotation effects.

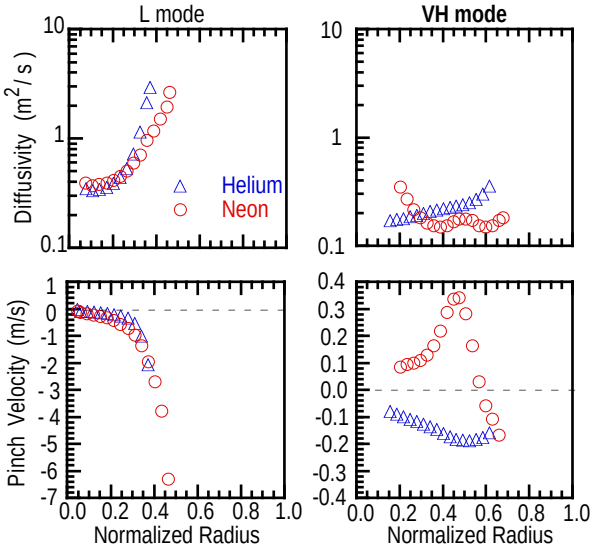

Fig. 3. Comparison of the transport coefficients for helium (Δ) and neon (o) in L–mode and VH–mode.

[1] Gohil, P.. et al., in Proc. of the 14th Symp. on Fusion Engineering, San Diego, California (IEEE, New York, 1992), Vol. 2, p. 1199.
[2] Perry, M.E., et al., Nucl. Fusion **31**, 1859 (1991).
[3] Allen, S.A., et al., J. Nucl. Mater. **220-222**, 336 (1995).
[4] Petrie, T.W., "Radiative Divertor Experiments in DIII-D with Deuterium Injection," submitted to Nucl. Fusion (1996).
[5] Kallenbach, A., et al., Nucl. Fusion **34**, 1557 (1994).
[6] Jackson, G.L., et al., Phys. Rev. Lett. **67**, 3098 (1991).
[7] Strait, E.J., et al., Phys. Rev. Lett. **75**, 4421 (1995).
[8] Wade, M.R., *et al.*, Phys. Plasmas **2**, 2357 (1995).
[9] Synakowski, E.J., et al., Phys. Fluids B **5**, 2215 (1993).